IFSCC 2025 full paper (abstract N° IFSCC2025-1732)

Assessing the impact of chronological aging on dermal blood and lymphatic microvasculature system using a 3D human endothelialized full-thickness skin model

Alexandre GABORIT[1*], Julie RORTEAU[2], Mikaëla BIGNARD[1], Kilian LAHO[2], Amélie THEPOT[2], Morgan DOS SANTOS[2]

[1] c.f.e.b SISLEY, PARIS, France
[2] LabSkin Creations, LYON, France

1. Introduction

In the skin, the dermal compartment supports different cutaneous structures as hair follicle, sebaceous glands, but also the cutaneous microvasculature. This vascular network ensures the supply of nutrients and oxygen to skin tissue, transports immune cells and plays an important role in thermoregulation mostly using vasodilatation and vasoconstriction functions **[1]**. With chronological aging, cutaneous microvasculature undergoes pronounced alterations affecting crucial functions, particularly dermal homeostasis and epidermal renewal **[2]**. In aged skin tissue, vessels density decreases, neovascularisation is reduced and vascular permeability increases. Due to the reduced number of vessels, the overall vascular network becomes disorganized resulting in a diminished exchange surface. This contributes to well-known signs of aging such as pallor, lower skin temperature and decreased microvascular reactivity **[2]**.

It has notably been demonstrated that changes in the extracellular matrix (ECM) driven by cellular senescence has a major impact on neovascularisation in older adults **[3][4]**. Indeed, the modifications of ECM composition observed during aging like disorganized collagen fibres and lack of elastin directly impaire the structure of vessels and neoangiogenesis. Moreover, ECM is a major growth factors reservoir and, because of the increased number of senescent cells, the production of these molecules is disturbed. As a consequence, microvascular network structure and maturation are impacted **[5][6]**.

2D culture cells, a simple and affordable model, routinely used for studying skin aging, lack the complex tissue-scale. Indeed, the complex skin structure and environment have a direct impact on cellular viability, morphology, mobility and differentiation **[7]**. Over the past few decades, numerous progresses have been made in *in vitro* three-dimensional (3D) skin models which

better reflect the complexity of human skin tissue. However, they usually fall short in capturing the intricate dynamics of cutaneous microvasculature in relation with the tissue microenvironment **[8][9]**.

To elucidate interactions between the ECM and endothelial cells in the context of aging, we developped a new functional 3D human aging skin *in vitro* model integrating microvascular systems. Aged endotheliazed skin equivalents (aESEs) were obtained by co-culturing in 3D aged human primary fibroblasts and keratinocytes with young human primary microvascular dermal blood and lymphatic endothelial cells in a scaffold made of collagen, glycosaminoglycans and chitosan under optimized cell culture conditions for ECM neo-synthesis as previously described **[10]**. As controls, young endotheliazed skin equivalents (yESEs) were obtained using only young human primary cutaneous cells. To decipher how dermal ECM aging impacts vascular-like structures formation, stability and maturity, structural modifications of the aESES constructs were analysed by histology and immunohistology. We also conducted morphometry analysis comparing aESEs to the yESEs controls.

2. Materials and Methods

2.1 Ethical considerations and human cutaneous cell isolation

Human skin tissue was collected according to the Declaration of Helsinki Principles and its use was declared to the French Research Ministry (declaration n° DC-2024-6232). A written informed consent was obtained from the donor according to the French bioethical law of 2014 (loi 94–954 du 29 Juillet 1994). Primary cultures of human fibroblasts, keratinocytes and endothelial cells were established from healthy skin biopsy obtained from young donor (< 5 years old – keratinocytes, fibroblasts and endothelial cells) or adult donor (> 50 years old – keratinocytes, fibroblasts). Normal human epidermal keratinocytes (NHEK), dermal fibroblasts (NHDF) and endothelial cells (HDMVEC) were isolated from human skin as previously described **[11]**.

2.2 3D endothelialized skin equivalent

The 3D full-thickness reconstructed skin model was obtained by co-culturing NHDF and HDMVEC in a scaffold made of collagen, glycosaminoglycans and chitosan during 28 days under optimized cell culture conditions for ECM neo-synthesis. NHEK were subsequently seeded on the top of the dermal equivalent constructs. After 7 days, skin equivalent were raised at day 35 at the air/liquid interface to allow the formation of the epidermal compartment. Skin equivalent samples harvested at day 49 of total cell culture were immediately fixed in neutral buffered formalin 4% (Diapath) for 24 h and embedded in paraffin or in OCT compound and frozen at −80°C, for histological and immunohistological analysis, respectively.

2.3 Histological analysis

To evaluate the global cutaneous structure of samples, haematoxylin-phloxin-saffron (HPS) staining was performed. Paraffin sections of 5 µm of each condition were cut. After dewaxing and rehydration, the samples were stained with HPS. After rinsing, the sections were dehydrated before the mounting of the slides with a hydrophobic mounting medium.

2.4 Immunohistological analysis

For immunohistochemistry on paraffin sections, after heat-mediated antigen retrieval treatment, non-specific binding was blocked in PBS containing 4% of BSA. Sections were then incubated with the primary antibody against collagen-I, CD31 and VE-cadherin diluted in PBS/BSA 4% overnight at room temperature. After incubation for 1 h with EnVision anti-mouse/rabbit-HRP secondary antibody (Dako EnVision^{+}, HRP), we applied DAB^{+} substrate solution to the sections to reveal the color of the antibody staining. Counterstained slides were obtained by immersing them in 25% Harris Haematoxylin counterstaining solution. As a negative control, primary antibody was replaced by the corresponding IgG class.

For immunofluorescence, after heat-mediated antigen retrieval treatment, non-specific binding was blocked in PBS containing 4% of BSA. Sections were then incubated with the primary antibodies against podoplanin diluted in PBS/BSA 4% overnight at room temperature. After incubation for 1 h with an AlexaFluor-568-conjugated anti-mouse secondary antibody (Molecular Probes, Invitrogen), nuclear counterstaining using DAPI was carried out routinely. As a negative control, primary antibody was replaced by the corresponding IgG class.

For hyaluronan detection, sections were incubated overnight with 3 mg/ml of biotinylated HA binding protein (HABP) (Merck). After washing with PBS, the bound HABP was visualized using avidin–biotin complex technique according to manufacturer's protocol (Vectastain® ABC-AP reagent ready-to-use detection system, Vector). Counterstaining was performed using Biebrich Scarlet, providing contrast to highlight tissue morphology. Sections were then rinsed, mounted, and imaged using brightfield microscopy.

2.4 Image acquisition

Immunostained specimens were observed using a Zeiss Axio Observer D1 microscope. Sixteen-bit images were saved in an uncompressed tagged image file format (tiff). Three representative images were captured for each condition in the same manner (n=9 in total).

2.5 Tissue morphometry analysis

Epidermal thickness

Epidermal thickness was obtained with a Euclidean distance map. Pixels corresponding to the epidermis were selected from other pixels. Images were converted to 8-bit binary image. Images corresponding to the area of interest were converted to a 16-bit distance map. To each epidermis pixel (nonzero) in the distance map binary image a value equal to its distance from the nearest background pixel (zero) was assigned. The epidermis basal line was selected and then applied on the distance map. The mean intensity of the basal line corresponds to the mean distance between the basal line and the *stratum corneum*. Data are expressed in µm.

Capillary diameters

Analysis of capillary-like structures was performed using ImageJ (NIH, USA). Circular or elliptical vascular-like profiles were automatically identified based on CD31 immunostaining and luminal appearance. The "Measure" tool was used to record the maximum (major axis) and minimum (minor axis) diameters for each structure. Structures showing clear lumens and a complete or near-complete endothelial-like boundary were included; collapsed or highly irregular profiles were excluded. At least 9 capillary-like structures per sample were measured. Surface area data were averaged for each sample to represent the mean capillary diameter expressed in μm^2.

Capillary cohesion

VE-cadherin expression was quantified by measuring the mean gray value of DAB staining. Images were analyzed using ImageJ (NIH, USA). Briefly, images were converted to 8-bit grayscale, and regions of interest (ROIs) corresponding to capillary-like structures were manually selected. The mean gray value (expressed in arbitrary units, a.u.; range 0 [black, strong staining] to 255 [white, no staining]) was recorded, with lower mean values indicating stronger DAB staining and thus higher VE-cadherin expression. For each sample, at least 9 fields of view were analyzed and averaged.

ECM-related markers quantification

For the markers of interest, positively red or blue stained-tissue areas were automatically detected and segmented from other pixels. Images were then converted in binary images, treated by mathematical morphology and sieved for isolating the regions of interest. The surface area of interest was measured automatically. Data were normalized by the total surface of dermal area. Data are expressed in percentage of density.

2.6 Statistical analysis

Statistical analysis was performed in R (R Foundation for Statistical Computing, Vienna, Austria), normality was checked using the Shapiro–Wilk normality test. The normal distribution led to a parametric test. Analysis of variance was performed using an ANOVA test, then the conditions were compared with each other using pairwise t tests as post hoc tests. The absence

of a normal distribution led to a non-parametric test. Analysis of variance was therefore performed using a non-parametric Kruskal-Wallis test, then the conditions were compared with each other using non-parametric Wilcoxon-Mann-Whitney test as post hoc tests. For all data, the statistical significance are indicated by asterisks as follows: *P < 0.05, **P < 0.01 and ***P < 0.001.

3. Results

3.1 Incorporation of aged donors-derived cutaneous cells in 3D skin model recapitulates changes typically associated with skin aging

The overall structure of 3D skin equivalent engineered with young (yESEs) and aged (aESEs) donor-derived cells were consistent at both epidermal and dermal levels. Histological analysis confirmed the formation of a pluristratified epidermis, well differentiated from the basal layer to the *stratum corneum*, anchored atop of the fibroblats-populated dermal equivalent enriched with newly synthesized ECM. Dermal-epidermal junction appeared cohesive and structurally regular in both models (Figure 1).

However, the incorporation of aged primary fibroblasts and keratinocytes in the 3D model led to tissue alterations that closely mimic intrinsic aging in both dermal and epidermal compartments. In aESEs, compared to yESEs, the epidermis had less layers of living cells. The terminal differentiation appeared to be disrupted, with less *stratum granulosum* impacting barrier function (Figure 1). Moreover, the extracellular matrix was less dense and abundant and showed signs of structural disorganization (Figure 1).

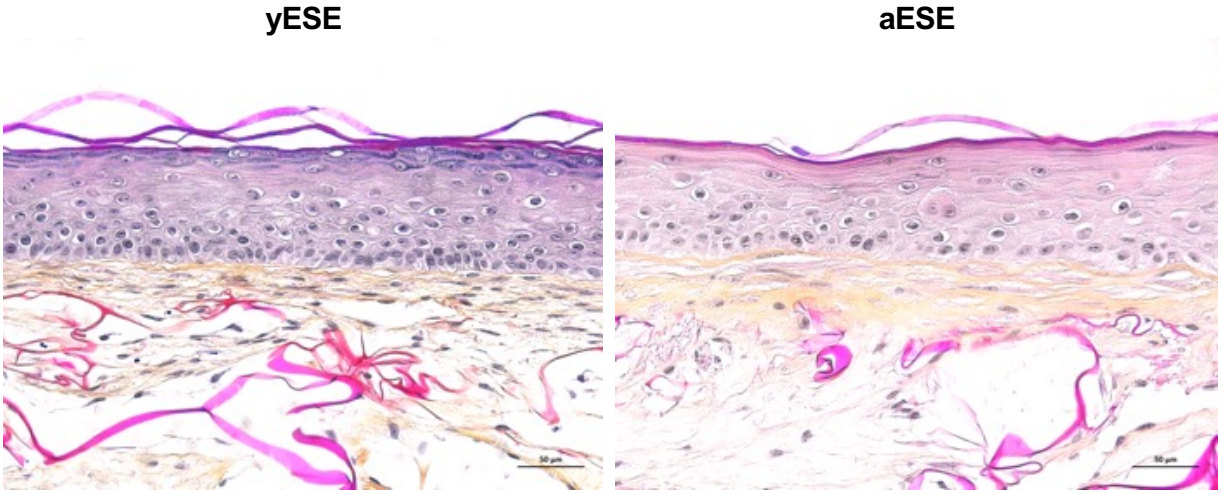

Figure 1. Histological analysis of endotheliazed skin equivalents (ESE) integrating human microvascular dermal endothelial cells. Representative images of histological analysis of young and aged endothelialized skin equivalents (yESE, aESE) of HPS staining. Scale bar: 50µm.

3.2 ECM-related markers drastically decrease in 3D aESE similarly to human aged skin

To further characterize the aging phenotype in the dermal compartment, the analysis of the three major ECM components, type I collagen, elastin and hyaluronan, was assessed by immunohistological analysis (Figure 2). It appeared that the expression of collagen I and elastin was significantly decreased in aESE compared to yESE. The fibres were less abundant, disorganized and fragmented, indicating a deterioration of ECM structure (Figure 2a). Similarly, hyaluronan levels were visibly decreased, suggesting impared ECM hydration and structural support. Collectively, these observations confirmed that dermal compartment was weakened by the presence of cutaneous aged cells in the 3D model. The ECM of aESE faithfully recapitulates key-related hallmarks of human aged skin.

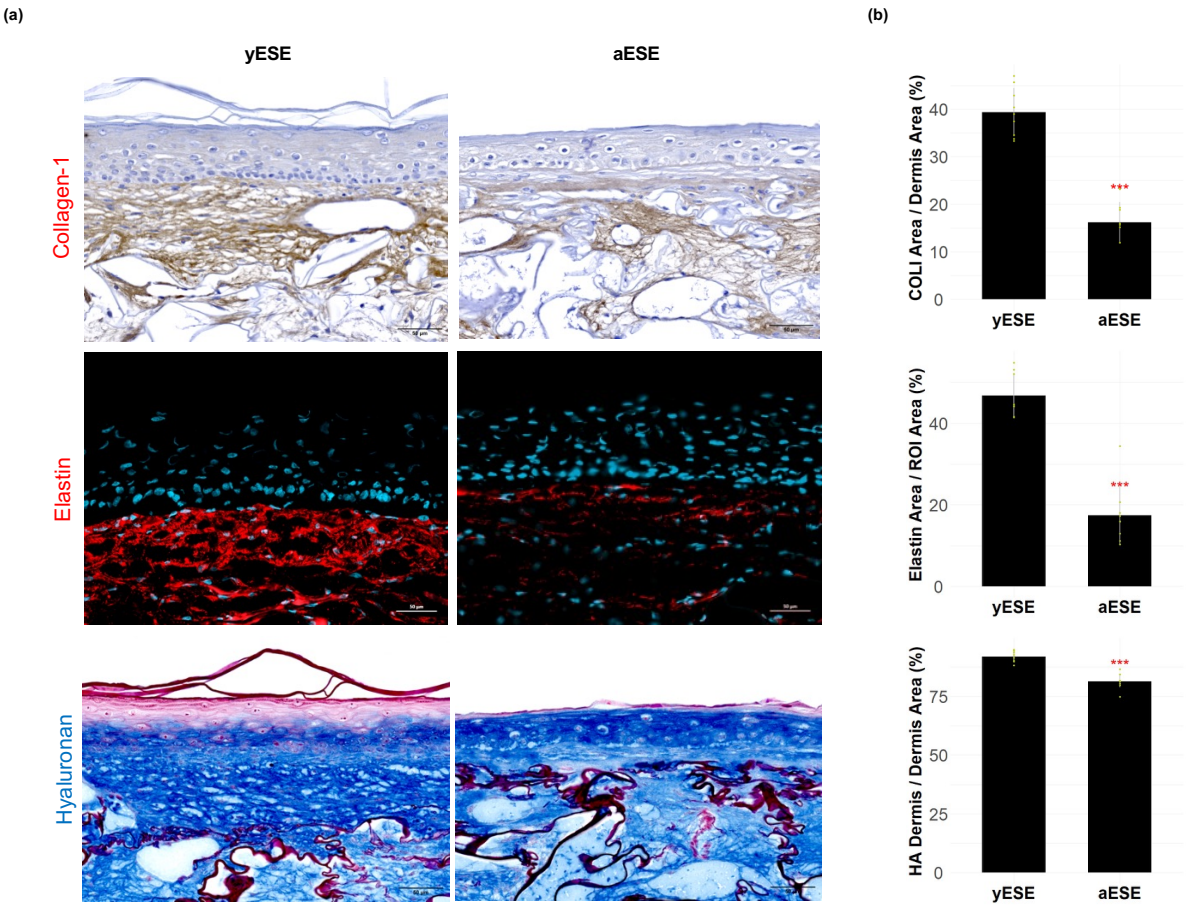

Figure 2. Immunohistological analysis of the main extracellular matrix components expressed in the 3D endotheliazed skin equivalents (ESEs). **(a)** Representative images of immunostainings of collagen-I (upper panel), elastin (mid-panel) and hyaluronan (lower panel) of young and aged endothelialized skin equivalents (yESE, aESE). **(b)** Immunohistomorphometry analysis of collagen I expression (upper chart), elastin expression (mide chart) and hyaluronan expression (lower chart) of the indicated conditions. Kruskal-Wallis test: *** $P < 0.001$. Scale bar: 50µm.

3.3. Aging alters capillary-like structure formation in the 3D skin model

Remarkably, capillary-like structures were observed in the dermal compartment of both yESE and aESE models (Figure 3). Immunostaining for CD31, an endothelial cell marker, demonstrated that endothelial cells successfully adhered, proliferated and organized into capillary-like ring structures embedded within the neo-synthetized ECM of both yESEs and aESEs (Figure 3a).

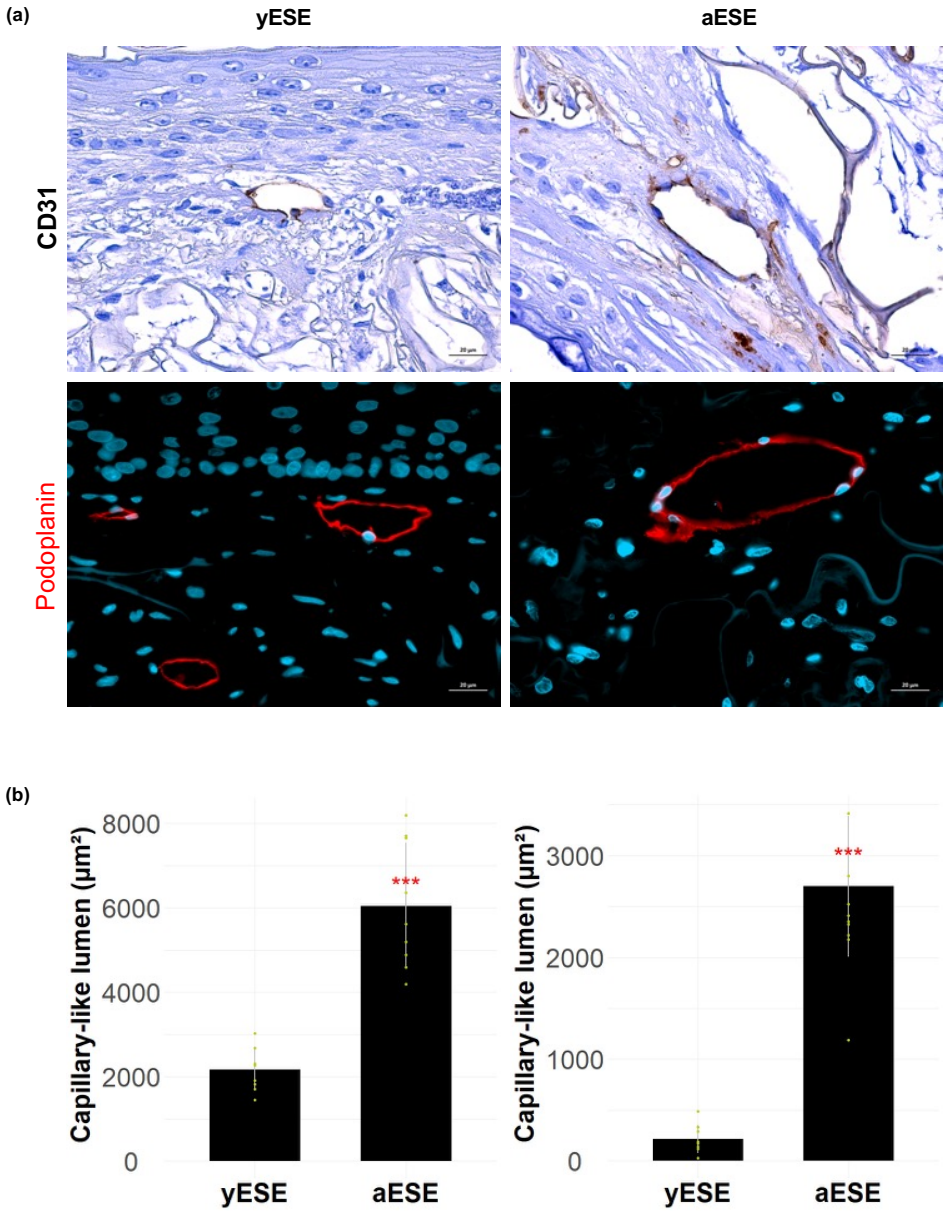

Figure 3. Immunohistological analysis of the capillary-related markers of the 3D aging endotheliazed skin equivalents (ESEs). **(a)** Representative images of CD31 (upper panel) and podoplanin (lower panel) expression of young and aged endothelialized skin equivalents (yESE, aESE). **(b)** Immunohistomorphometry of capillary-like lumen diameter of global vasculature based on CD31-positive signal (left panel) and lympatic vaculature based on podoplanin expression (right panel). Kruskal-Wallis test: *** $P < 0.001$. Scale bar: 20µm.

In addition, this ECM microenvironment also supporteded the proliferation and the formation of lymphatic capillary-like structures as demonstrated by the immunostaining of podoplanin, a protein expressed specifically by lymphatic endothelial cells (Figure 3a).

However, a notable difference was observed in the morphology of these vascular structures between the two models. For both blood and lymphatic capillary-like structures, the lumen surface area in aESEs was significantly enlarged compared to the ones observed in yESEs (Figure 3b). The capillary-like structures appeared looser than those observed in the young control, suggesting impaired vascular organisation in the 3D skin model; a known feature of aged skin.

3.2. Aging reduces vascular density and impairs vascular organization in the 3D skin model

In addition to morphological alterations in capillary-like structures, the aESE model exhibited a significant reduction in vascular density. Numerous oblitered or collapsed vessels were also observed, particularly within the upper dermal areas, indicating the negative impact of aging on global capillary-like structure. Immunohistochemical analysis further revealed a marked decrease in VE-cadherin expression in aESEs relative to yESEs (Figure 4). VE-cadherin, a critical component of endothelial adherens junctions, is essential for maintaining vascular barrier function and endothelial cohesion. In the aged model, VE-cadherin staining appeared not only weaker but also significantly thinner (Figure 4a-b), suggesting reduced junctional continuity. These alterations are consistent with an increase in vessel permeability, a hallmark of aging-related vascular dysfunction.

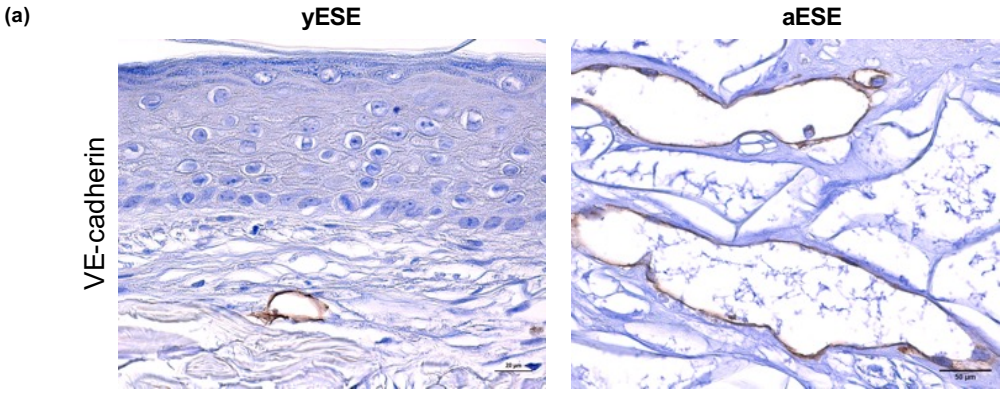

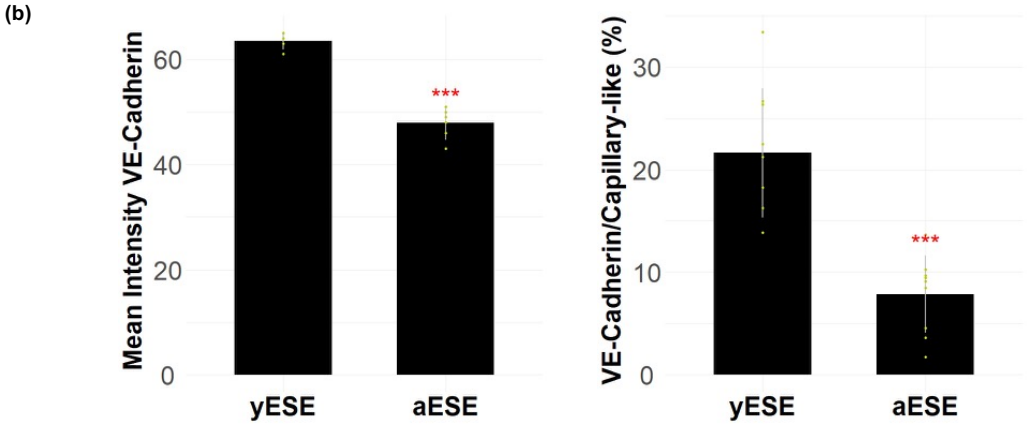

Figure 4. Immunohistological analysis of the endothelial permeability VE-cadherin expression of the 3D aging endotheliazed skin equivalents (ESEs). **(a)** Representative images of VE-cadherin immunostaining of young and aged endothelialized skin equivalents (yESE, aESE). **(b)** Immunohistomorphometry of VE-cadherin expression based on the mean grey value (left chart) and the surface area (right panel). Kruskal-Wallis test: *** $P < 0.001$. Scale bar: 20µm.

4. Discussion

To date, very few 3D skin models have enabled detailled analysis of cutaneous microvasculature despite its essential role in maintaining skin homeostasis and its progressive deterioration during aging **[12]**. Most aging-focused *in vitro* systems fail to integrate functional endothelial networks, largely due to technical challenges such as the co-culture of different cell types and the difficulty of sustaining complex models long enough to allow analysis of aging responses **[9]**. Here, we successfully developed a new full-thickness 3D skin model incorporating human primary microvascular dermal blood and lymphatic endothelial cells capable of forming capillary-like networks within a neosynthesized ECM. Notably, we showed that this vascular compartment responds to aging stimuli, making it a valuable model for studying microvascular aging in a controlled and physiologically relevant context. When we used endothelial cells obtained from young individual in both young and aged endotheliazed skin equivalents, the vascular-like structures obtained were very different. These results demonstrated that, as in human skin, the formation and maturation of the microvascular compartment is influenced by the dermal microenvironment **[5]**. In the aESEs, the blood and lymphatic vascular-like structures were less numerous and presented enlarged lumen area meaning that the aged ECM of this skin equivalent failed to support the formation of correct vascular structures. Crucially, in this innovative model we also observed a thinner immunostaining of VE-cadherin directly linked to the permeability of cutaneous microvessels suggesting an hyperpermeability of the structures formed in the aged microenvironment compared to the young one.

Together, these data highlight the bidirectional interplay between the extracellular matrix and endothelial cells during aging and emphasize the importance of developing advanced models

that account for vascular and matrix dynamics. Our model bridges this gap and provides a reproducible platform for exploring not only microvascular aging but also the effects of anti-aging or pro-angiogenic treatments in a physiologically relevant context.

5. Conclusion

This study demonstrates that dermal ECM aging critically affects the formation, stability, and permeability of the skin microvasculature, even in the presence of young endothelial cells. Using a novel 3D skin model that integrates blood and lymphatic endothelial networks, we reproduced key aging-related changes such as reduced vascular density, lumen enlargement, and increased permeability, all driven by the aged cutaneous microenvironment.

Our findings underscore the crucial regulatory role of dermal ECM composition and organisation in shaping the structural stability and maturity of the cutaneous vascular system during aging using a 3D skin model. This work provides not only a valuable experimental model for understaining skin vascular aging but also a foundation for evaluating new strategies targeting aging-related changes in matrix components to restore microvasculature homeostasis affected by aging.

This innovative model paves the way toward the rational development of anti-aging compounds capable of preserving or regenerating the vascular network, offering potential benefits for both dermatological therapies and advanced cosmetic applications.

[1] Johnson JM, *et al.* Compr Physiol. 2014 Jan;4(1):33-89.
[2] Rorteau J, *et al.* Med Sci (Paris). 2020 Dec;36(12):1155-1162. French.
[3] Xiao P, *et al.* J Transl Med. 2023 Jul 11;21(1):457.
[4] Gunin AG, *et al.* Exp Gerontol. 2014 Jul;55:143-51.
[5] Jacob MP. Biomed Pharmacother. 2003 Jul-Aug;57(5-6):195-202.
[6] Jacob MP. Med Sci (Paris). 2006 Mar;22(3):273-8. French.
[7] Jensen C, *et al.* Front Mol Biosci. 2020 Mar 6;7:33.
[8] Lombardi F, *et al.* Biomolecules. 2024 Aug 26;14(9):1066.
[9] Sanchez MM, *et al.* Aging (Albany NY). 2022 Nov 22;14(22):9338-9383.
[10] Black AF, *et al.* Tissue Eng. 2005 May-Jun;11(5-6):723-33.
[11] Germain L, *et al.* Burns. 1993 Apr;19(2):99-104.
[12] Rimal R, *et al.* Adv Healthc Mater. 2024 Apr;13(9):e2303351.